Crosslinking Mechanisms, Structure and Glass Transition in Phthalonitrile Resins: Insight from Computer Multiscale Simulations and Experiments

D. V. Guseva,[1] **V. Yu Rudyak**,[1] **P. V. Komarov**,[2,3] **A. V. Sulimov**,[4] **B. A. Bulgakov**,[4,5] **A. V. Chertovich**[1]

[1]Faculty of Physics, Lomonosov Moscow State University, Leninskie Gory, 1-2, Moscow 119991, Russia
[2]Department of General Physics, Tver State University, Sadovyj per., 35, Tver 170002, Russia
[3]Nesmeyanov Institute of Organoelement Compounds, Russian Academy of Sciences, Vavilova st., 28, Moscow 119991, Russia
[4]Institute of New Carbon Materials and Technologies, Leninskie Gory, 1-11, Moscow 119991, Russia
[5]Faculty of Chemistry, Lomonosov Moscow State University, Leninskie Gory, 1-3, Moscow 119991, Russia
Correspondence to: D. V. Guseva (E-mail: Darya.Guseva@gmail.com)

Received 29 July 2017; accepted 7 November 2017; published online 00 Month 2017
DOI: 10.1002/polb.24548

ABSTRACT: The influence of crosslinking process on the resulting structural properties of phthalonitrile matrices is studied through theoretical and experimental investigations. Multiscale procedure for generating fully atomistic phthalonitrile networks with simulation of radical polymerization reactions and specific reactions of triazine formation at the mesoscale level is presented and applied to the case of phthalonitrile resin based on low-melting monomer *bis(3-(3,4-dicyanophenoxy)phenyl)-phenyl phosphate*. The structural properties of the generated networks of various conversions and with various amount of triazine are analyzed using the dissipative particle dynamics and atomistic molecular dynamics. Triazine-containing networks are much sparser in comparison with triazine-free ones in terms of simple cycle size. The values of density, coefficients of linear thermal expansion and glass transition temperatures (T_gs) agree with obtained experimental data, and are very similar for different crosslinking mechanisms. The dependence of T_g on conversion correlates well with the sol–gel transition in network structure. © 2017 Wiley Periodicals, Inc. J. Polym. Sci., Part B: Polym. Phys. **2017**, *00*, 000–000

KEYWORDS: crosslinking; dissipative particle dynamics; glass transition; matrix; modeling; molecular dynamics; phthalonitriles; structure

INTRODUCTION Temperature range for composite applications is limited by polymer matrix. Carbon fiber reinforced polymers with common matrices for high-temperature applications, such as bis-maleimides[1,2] and polyimides,[3–5] are stable up to 300 °C. High-performance polymer matrices for use at temperatures above 400 °C and capable of retaining their (thermal, chemical, electrical, and mechanical) properties under influence of various destructive factors may be produced from low-melting phthalonitriles.[6–8] The usual phthalonitrile monomer consists of two phthalonitrile fragments linked by various aromatic rings. However, in most of the previous works, synthesized phthalonitrile matrices had high curing temperature and narrow processing temperature range.[8–11] Recently, it was shown[8,11–13] that the modification of phthalonitrile monomers with silica or phosphate bridges reduces glass transition temperatures T_gs of the monomers and increases processing window. At the same time, a thorough study of the effective processing of these monomers using experimental methods is still time consuming, expensive and limited due to the need of taking into account their structural changes during reaction. Computer simulations provide a tool of direct examining how chemistry of constituent monomers and reaction kinetics influence macroscopic material properties. In our recent papers,[11,14] a systematic study of a set of industrially important phthalonitrile monomers was carried out using molecular dynamics simulations. We estimated their T_gs and found a good agreement with experiments. The bulks of monomers with larger residues tend to have higher T_gs, while compounds with longer silica bridges have lower T_gs. We also analyzed local monomer dynamics during glass transition, and found two factors that influenced the relaxation mechanisms: energetic, provided by rigidity of molecules, and entropic, connected with available volume of conformational space. In this paper, we try to understand the relationship of physical properties to crosslinking process using a multiscale approach. We use coarse-grained (the dissipative particle dynamics (DPD))[15,16] and Monte Carlo methods for simulation of crosslinking process of phthalonitriles and topological analysis of the resulting networks, and atomistic molecular dynamics for calculating

their structural properties. The structural analysis of the corresponding experimental samples is additionally carried out. These results, we believe, are required for effective industrial synthesis of phthalonitrile matrices.

In previous works,[17–28] a variety of computational methods of polymer network formation have been developed. These methods were capable to study and reproduce thermomechanical properties of realistic polymer (epoxy and elastomer) networks. Simulation of crosslinking reactions in these works was implemented either at atomistic level[17–19] or using coarse-grained (multiscale) approach.[20–28] Yarovsky and Evans[17] developed a static crosslinking method, in which all of the bonds were created simultaneously at a one step. In other works,[18,19] new covalent bonds were created stepwise, and, in the work of Wu and Xu,[19] were followed by some iterative molecular-dynamics (MD) relaxation simulations. In the work of Heine et al.[18] a free end and crosslinker could react when approaching within a capture distance.

Although chemical reactions can be modeled directly, using atomistic molecular dynamics and "reactive force field" (ReaxFF),[29,30] this method cannot be used for obtaining large atomistic models of crosslinked polymers. This is because the kinetics of reactions is controlled by the diffusion rates of the reactants. As degree of conversion increases, diffusion of monomers is drastically decelerated, and to obtain highly crosslinked systems (with higher conversion degree) one have to perform simulations on very large time intervals. This is aggravated by the fact that the use of ReaxFF slows down the total simulation speed in about 10–50 times in comparison with the use of conventional (non-reactive) force fields.

To overcome the limitations imposed by the atomistic MD coupled with ReaxFF, it is convenient to simulate the polymerization reaction basing on coarse-grained (CG) models.[22,24–28] In these models the reduction of the degrees of freedom by removing detailed information about the chemical structure makes it possible to achieve higher mobility of monomers and to increase the total simulation rate of the reaction of crosslinking. This is why we believe that simulation of the polymerization reaction on the mesoscopic level is the only way of constructing models for highly crosslinked polymer materials.

In this paper, to create full atomistic models of crosslinked matrices we used a multi-step approach with simulation of chemical reaction of crosslinking at the mesoscale level (construction of coarse-grained models for initial monomers → simulation of polymerization in the coarse-grained representation → reverse mapping of coarse-grained matrices onto fully atomistic representation → simulation of the atomistic network using molecular dynamics method) that was originally formulated in the work of Komarov et al.[22] and then modified in the work of Gavrilov et al.[25] for simulating the formation of highly crosslinked epoxy polymer networks. In ref. 22 network formation and relaxation was performed by Monte Carlo simulations, while in ref. 25 to simulate crosslinking process the DPD method and probabilistic reaction scheme were used. This multiscale computational method makes it possible to create well-relaxed highly crosslinked atomistic networks and to predict their thermo-mechanical and structural properties. The similar four-step multiscale strategy was used by Liu et al.[23] The authors[25–27] also showed that for obtaining reasonable local structure of an epoxy network the simulation box should be rather large (no less than $150 \times 150 \times 150$ A^3 for the studied resin). In ref. 31, the DPD method was suggested for simulation of crosslinking process of phthalonitrile monomers with specific reactions of isoindoline and triazine formation.[32–35] In this paper, we generalized the scheme from refs. 22 and 31 to take into account all features of the system under simulation and to generate fully atomistic phthalonitrile networks.

Crosslinking significantly change the physical properties of polymers, in particular, T_g, either increasing[36–41] or decreasing[42,43] it. Most existing experimental[38,39] and theoretical[40,41] results confirm that T_g increases with crosslinking. Nielsen[36] considered that topological constraints caused by crosslinks increase T_g, while copolymer effect may either increase or decrease T_g, depending on chemical nature of polymer and crosslinking agent. Shefer and Gottlieb[37] reviewed that the increase in T_g may be associated with several effects: reduction of the concentration of chain ends, which is believed to be the most important in the formation of thermosets and end-linked networks; "plasticizer effect" that is disappearance of small molecular weight molecules; formation of branch points and crosslinks; non-Gaussian chain statistics, affecting highly crosslinked networks; and the formation of cyclic structures. Recently Lan et al.[44] performed MD simulation of crosslinking process of propellant binder and showed that T_g mainly depended on the motions of the molecules and freedom space and that the conformational change of highly crosslinked molecules was "frozen out." Thus, T_g of crosslinked network is higher due to corresponding restriction of molecular relaxation.

A variety of novel phthalonitrile materials with enhanced thermal and mechanical properties, with[32] and without[33] triazine have been synthesized recently. Yang et al.[32] showed that the formation of phthalocyanine rings and triazine rings through crosslinking led to the enhancement of thermal, mechanical, and dielectric properties. However, understanding of T_g dependence on the reaction regime and formation of phthalocyanine rings or/and triazine rings is still lacking, and, to the best of our knowledge, was not investigated by computer simulation methods. In this paper, we performed the structural analysis of polymer matrices with and without triazine and of various degrees of conversion. We calculated the maximal cluster size and the distribution of simple cycle lengths[25] through DPD simulations and the system density during glass transition using MD simulations. NMR analysis and structural measurements of the corresponding experimental samples were also carried out.

Thus, the aim of this paper is to develop multiscale procedure for generating fully atomistic phthalonitrile networks

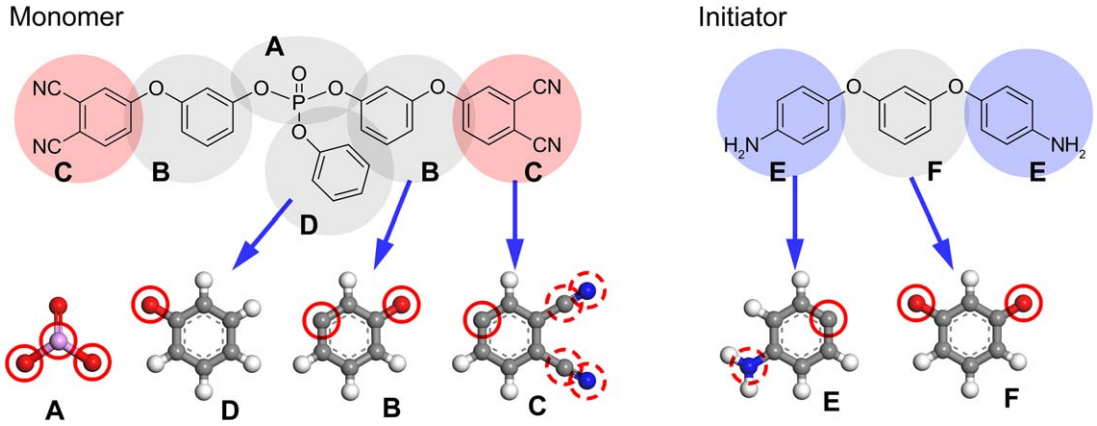

FIGURE 1 Upper pictures: chemical structures of phthalonitrile monomer *bis(3-(3,4-dicyanophenoxy)phenyl)phenyl phosphate* (**1**) and initiator (diamine curing agent APB) with their coarse-grained mapping schemes. Six different types of coarse-grained particles are used: A, B, C, D, E, and F. Lower pictures: the initial atomistic structures that correspond to each type of coarse-grained particles. Atoms are colored according to the atom types: hydrogen atoms are shown in white, carbon atoms are shown in gray, oxygen atoms are shown in red, nitrogen atoms are shown in blue, phosphorus atom is shown in magenta. Passive RA are marked with solid red circles, active RA – with dashed red circles. [Color figure can be viewed at wileyonlinelibrary.com]

(with the possibility of forming triazine, which mimics processes of high-temperature and low-temperature crosslinking), to validate this procedure on the polymer matrices of specific phthalonitrile monomer and to predict how the monomer chemistry and the way of processing and crosslinking influence the properties of the resulting composite using theoretical and experimental observations. We believe our results will contribute to the effective industrial synthesis of future high-performance phthalonitrile materials.

METHODOLOGY DEVELOPMENT

DPD Coarse-Graining Scheme

We used dissipative particle dynamics simulations to simulate matrix curing at the mesoscale level and to obtain equilibrated network structures of standard phthalonitrile resin based on monomer *bis(3-(3,4-dicyanophenoxy)phenyl)phenyl phosphate* (**1**) and diamine curing agent (APB) as an initiator (see Fig. 1). DPD is a mesoscale simulation technique suggested by Hoogerbrugge and Koelman[15,16] for studying the behavior of highly dispersed particles in a flow and later developed for simulations of polymers and molecular systems.[45–47] The integration step of the equations of motion in DPD is several times larger than those in molecular or Brownian dynamics, which makes it possible to model large-scale systems that contain hundreds of thousands of particles, including highly crosslinked polymer networks. In DPD molecular systems (polymer chains) are represented as soft particles (beads), connected by harmonic springs. The evolution of these beads is described by Newton's equations. The beads interact through the conservative repulsive forces proportional to repulsion parameters a_{ij} (connected to the Flory–Huggins χ-parameters as $a_{ij}=25+3.497\chi_{ij}k_BT$, $i\neq j$, where k_B is the Boltzmann constant),[46] the retarding (dissipative) and stochastic forces, which provide the temperature control of the system and account for the hydrodynamic interactions between the beads. Recently this method was successively adopted for simulating chemical reactions by the concept of "mesoscale chemistry."[25,31,48] In our approach the modified version of DPDChem software is used.[49]

To create a correct topology of highly crosslinked network of monomers in the course of CG simulation, it is necessary to choose an adequate scheme of coarsening of the initial monomers at the stage of the CG model design.[50,51] This coarse-graining scheme involves retention of information about the excluded volume of the initial molecules and general features of the intermolecular interactions. This is important for producing well-equilibrated CG system, that in turn will reduce the total time expenses on the subsequent relaxation of the atomistic model.

In our approach coarse-grained bead-spring model of the initial components is based on their molecular structure. The scheme of the direct mapping of initial chemical structures into the coarse-grained representation is shown in Figure 1. Six different types of coarse-grained particles are used: A, B, C, D, E, and F. For the correct description of curing reactions, the additional marks can be assigned to the particles C and E (see *Simulation of curing process* section). All beads consist of benzene rings with one or two groups attached and, thus, have near the same molecular mass and excluded volume (excepting the central bead A that substitutes phosphorus bridge). The constructed CG molecules of monomer and initiator are composed of 6 or 3 CG particles, respectively (see upper pictures of Fig. 1). As in this CG structure of molecules the areas of potential molecular flexibility are fitted with bonds between beads it is also convenient for the subsequent construction of the atomistic model using the reverse mapping procedure.

According to the mapping scheme of the initial atomistic structures of monomer and initiator onto the coarse-grained representation in Figure 1, each of CG particles is capable of

establishing one or two intermolecular bonds which are introduced between their centers. The newly formed covalent bonds are introduced between so-called reactive atoms (RA).[22] The reactive atoms are classified into passive and active ones. The passive RA (marked with solid red circles on lower pictures of Fig. 1) are used for building CG models of initial molecules. They depict the atoms, which are already connected by covalent bonds in the initial monomers. This information is very important for correct functioning of the reverse mapping procedure (see *DPD → MD reverse mapping* section). In turn, the active RA (marked with dashed red circles on lower pictures of Fig. 1) are used for introducing new chemical bonds that arise between the pairs of CG particles during the simulation of chemical reactions (see *Simulation of curing process* section).

In our study, the simulation box had size $10 \times 10 \times 10$ DPD units. For example, for the system without triazine of conversion 0.1 at $T = 300$ K it corresponds to approximately $7.4 \times 7.4 \times 7.4$ nm^3, which was recently shown to be large enough for this compound to contain representative part of the network.[31] At the beginning, it was randomly filled with monomer and initiator molecules in mass proportion of 96:4, that corresponds to 480 monomers and 40 initiator molecules. The interaction parameters in DPD model are described in the *Choosing DPD interaction parameters* section.

Simulation of Curing Process

Phthalonitrile resins are formed from melt by radical polymerization reaction, accompanied by more complex reactions of triazine and phthalocyanine formation.[34,35] In this paper, curing process with multiple reactions, that mimics actual chemical reaction pathways, is implemented at the mesoscale level.[31] For this purpose, the ending beads of each molecule are being assigned with valence (amount of new covalent bonds that the particle can form) and active center (particle that contains initiating group or radical atom) marks:

- ending bead of the initiator molecule (E on Fig. 1) has valence equal to one and is marked as active center (E*, see Fig. 2);
- ending bead of the valence monomer (C on Fig. 1) has valence equal to two.

To take into account specific chemical transformations additional marks to particle C are also being assigned (C′*, C″*, C′, C″, see Fig. 2). During the simulation of curing process the following chemical reactions are allowed:

1. Initiation reaction, when initiator molecule and monomer molecule form a bond and the corresponding monomer particle transforms to isoindoline with radical atom N (see (**a**,**b**) on Fig. 2). The initiation reaction consists of two steps. At the first step (see (**a**) on Fig. 2), when the ending bead of initiator (E* on Fig. 2) reacts with the ending bead of monomer (C on Fig. 2) the nitrile group of the C bead discloses and the C bead becomes an active site in an intermediate state (C′* on Fig. 2). At the second step (see (**b**) on Fig. 2), this intermediate state transforms into isoindoline (C″* on Fig. 2). After the formation of the new bond between the monomer and the initiator, the active center mark (asterisk in Fig. 2) is passed on the C bead.
2. Simple polymerization reaction, when an active site forms a new bond with a neighboring terminal bead with available valence and passes the active state to that bead, see (**c**,**d**) on Figure 2. As a result a sub-chain of polymer network is formed. The mechanism of simple polymerization reaction is similar to that of initiation reaction: when an active site C″* of the monomer reacts with a neighboring terminal bead C the nitrile group of the C bead discloses and the C bead becomes an active site in an intermediate state (C′*, see (**c**) on Fig. 2), which transforms then into isoindoline (C″*, see (**d**) on Fig. 2).
3. Triazine formation reaction, during which three adjacent terminal beads in the intermediate state consequently link with each other and finally form a triple link, see (**e–h**) on Figure 2. First, an active site in an intermediate state C′* react with a neighboring terminal bead C, the nitrile group of the C bead discloses and the C bead becomes an active site in an intermediate state (C′*, see (**e**,**f**) on Fig. 2). After these two adjacent terminal beads link with each other, the active center mark is passed on the second terminal bead. Then, similarly, these two adjacent terminal beads link with the third terminal bead (see (**g**) on Fig. 2). The first of these three terminal beads detaches from the preceding chain of terminal beads and retains three bonds in sum, which is dictated by the details of the chemical reaction (see (**h**) on Fig. 2).

The initiation reaction and simple polymerization reaction are carried out probabilistically. At regular time intervals, a pair of reactive atoms – an initiator terminal bead/active terminal bead and adjacent terminal beads with free valences – when approach at a reaction radius $R_c = 1$ form a new bond with the probability $p = 0.01$, which is small enough to keep quasi-equilibrium conditions in a vicinity of reaction centers.[48] Triple link formation is performed with the same periodicity for each triplet of terminal beads, that ends with active site. For simplicity, reaction steps (**b**) and (**d**), effectively converting C′* to C″* and C′ to C″, are produced in the end of simulations for all C′* sites and all C′ sites, which are not forming triazine cycle. This is why the probability of triple link formation, p_t, defines the ratio between the reaction rates of simple and triple link reactions.

In experiments the ratios between reaction rates of these reactions can be controlled by chemical structure of reactants and temperature regime (but are still unknown).[33,35] In simulations two-stage process is implied to simulate the actual technological curing procedure. On the first stage, low-temperature regime with $p_t = 0$ is simulated. This stage continues until the percolation cluster occurs. After the percolation, the second stage of the curing process is simulated. It can be produced either in the same low-temperature regime ($p_t = 0$) or in high-temperature regime ($p_t = 1$).

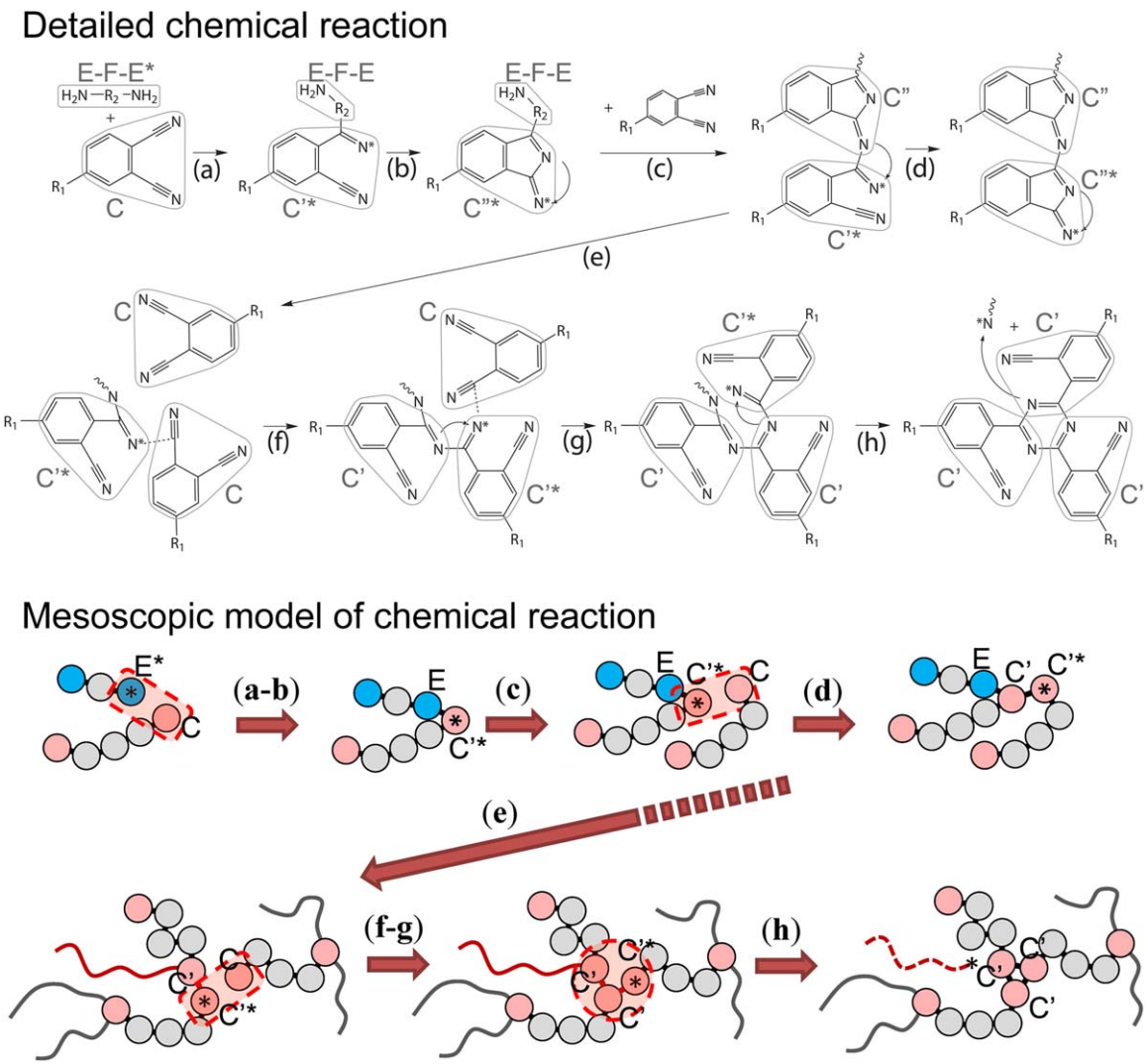

FIGURE 2 The detailed scheme of chemical reaction (upper picture) and the scheme of chemical reaction in mesoscopic model (lower picture): (a,b) initiation reaction; (c,d) simple polymerization reaction; (e–h) triazine formation reaction. Active sites are marked with asterisk. [Color figure can be viewed at wileyonlinelibrary.com]

Reaction probability $p_t = 0$ leads to absence of triazine formation during the simulations. Reaction probability $p_t = 1$ leads to the maximum amount of triazine formed during polymerization reactions. It should be noted, that differences between the matrix properties at $p_t = 0$ and $p_t = 1$ are expected to overestimate experimental differences between low- and high-temperature regimes, and are intentionally calculated for demonstrating the maximum possible shift of the matrix properties. The real experimental rates at high-temperature curing regime are uncertain and lay somewhere between these numbers.

DPD → MD Reverse Mapping

The resulting CG samples contain a skeleton model of cross-linked polymer matrices and are used as *input* to our reverse mapping procedure.[22] This procedure extracts the following information of the final state of the CG system, viz, types of coarse-grained particles, their coordinates and all bonds between them (intra-monomer and newly formed). The implementation of the reverse mapping procedure is performed as follows (see Fig. 3):

Step 1: The cubical simulation cell with the edge length of $L' = KL$, where $K = (M/\rho)^{1/3}/L$ (L is the edge length of the CG simulation cell, M is the total mass of the atomistic model, and ρ is its density) is being built. Thus, the size of the CG system is scaled by the choice of density of the final atomistic system. The value of density ρ is chosen to be equal to 1 g/cm^3 that is a bit less than the experimental one (see Table 1). Such choice makes it possible to reduce the probability of a spatial overlap of atoms and spearing of benzene and triazine rings by bonds of the closely spaced monomers. The value of K is also used for the scaling of the coordinates of the CG particles $\{\mathbf{r_i}\} \rightarrow \{K\mathbf{r_i}\}$. All CG particles are sequentially replaced by corresponding atomistic models. During this process, coordinates of CG particles are assigned

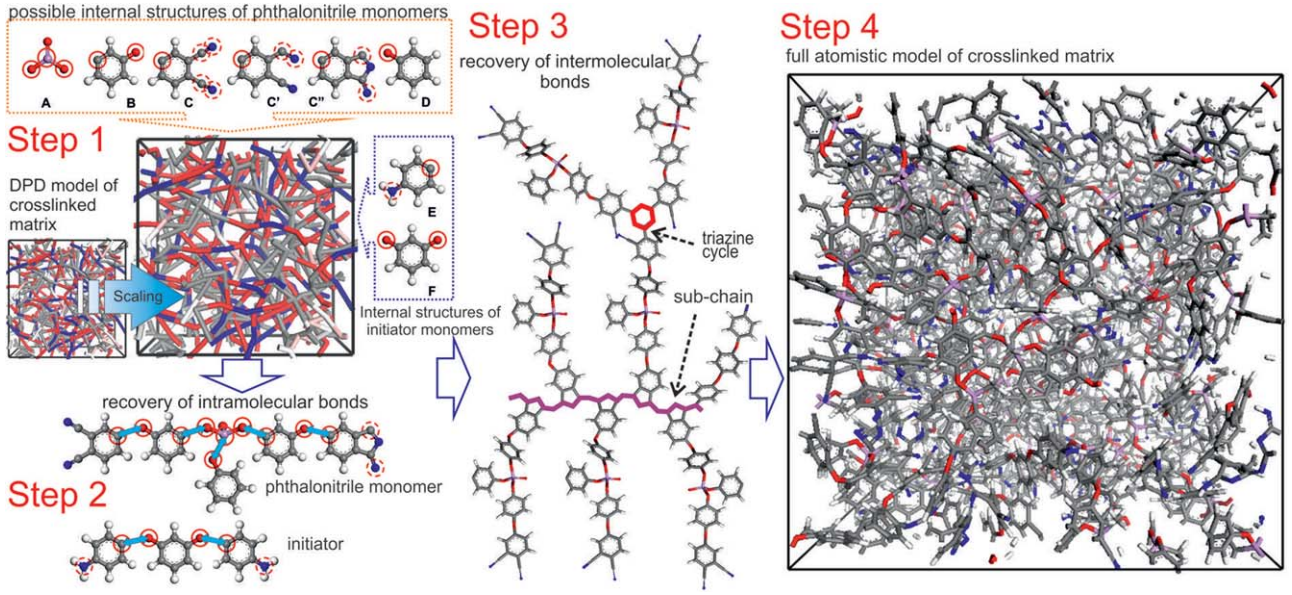

FIGURE 3 The scheme of the reverse mapping procedure. *Step 1*: Scaling of CG model of crosslinking system (to achieve a target density) and substituting of all monomers according to their internal state obtained in the course of the chemical reaction (see Fig. 2). *Step 2*: The intramonomer chemical bonds are established between all passive RA according to the atomistic models of monomers (see Fig. 1). *Step 3*: The intermonomer chemical bonds are established between all active RA according to the CG skeleton model of a crosslinked polymer matrix used and all free valences in the system are filled with hydrogen atoms. *Step 4*: The distances between all reaction atoms are readjusted using the MC procedure. [Color figure can be viewed at wileyonlinelibrary.com]

to centers of mass of atomistic structures (see Figs. 1 and 3). The chemical bonds are established between all RA according to the CG skeleton model of a crosslinked polymer matrix used.

Step 2: All passive reactive atoms are linked to restore the internal structure of all monomers and initiator molecules according to their chemical transformations during the chemical reaction. The bonds within the monomers, that correspond to the C particles, connected in isoindoline chain, (C″*, C″ on Figs. 2 and 3) are edited to form 2H-pyrrole rings. Then, to minimize the bond lengths between the passive RA their orientation is adjusted using a simple Monte Carlo procedure (all distances between the atoms in the monomers are fixed).[22]

Step 3: The active RA atoms are bonded according to the topology of CG model. More precisely, at this stage the bonds between the active RA of the monomers C″—C″ and C″—C″* (Fig. 2) are introduced and sub-chains of polymer network are formed (Fig. 3). The C particles connected into triple links (C′C′C′-ring, see (**h**) on Fig. 2) are edited to form triazine ring (see Fig. 2). After that, all remaining free valences of RA are saturated with hydrogen atoms.

Step 4: Finally, the distances between all reaction atoms are re-minimized using the MC procedure.

When the reverse mapping procedure is completed, the restored matrix may contain the so-called spearing monomers. They may be formed due to spearing of benzene rings by inter-atomic bonds of the closely situated pairs of monomers. Such misalignments in matrix structure are identified and eliminated using our specially written Monte Carlo based procedure that detects the spearing pairs and eliminates them by relocating and rotating molecular fragments. Then, initial MD equilibration is performed (the details of the MD simulations are described below).

Choosing DPD Interaction Parameters

We start from the assumption that since we simulate a high-temperature reaction (when the entropy contribution to the

TABLE 1 The Values of Density at Normal Conditions, CLTE and T_g Obtained Experimentally for Various Curing Temperatures

Curing Temperature (°C/K)	Density (g/cm^3)	CLTE (10^{-5}·K^{-1}) and the Temperature Range of Its Determination (in Brackets)	T_g (°C/K)
200/473	1.3585 ± 0.0013	5.88 ± 0.12 (40–90 °C/313–363 K)	121/394 ± 4
250/523	1.356 ± 0.003		196/469 ± 4
300/573	1.362 ± 0.002	5.89 ± 0.12 (40–180 °C/313–453 K)	325/598 ± 4
350/623	1.3908 ± 0.0009	4.19 ± 0.08 (50–280 °C/323–453 K)	416/689 ± 4

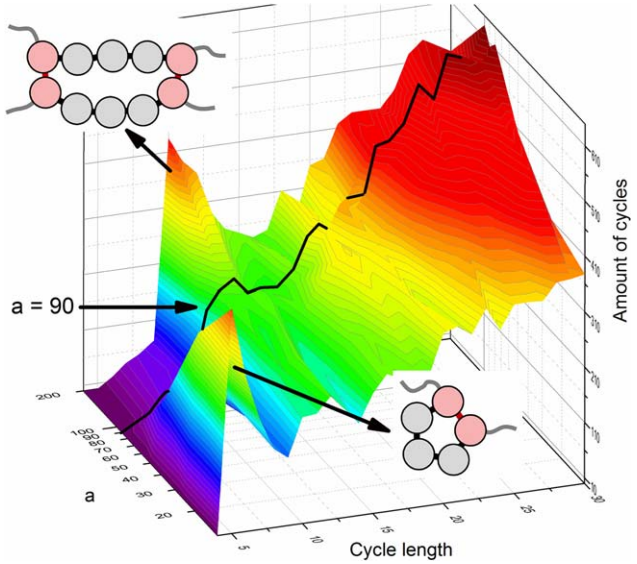

FIGURE 4 Part of distributions of simple cycle lengths with the small cycle length for matrices cured with various interaction parameters ($b = a$, $c = 0.02a$). Conversion degree equals to 0.9 for each value of a. Thick black line corresponds to the distribution of the simple cycle lengths at the optimum choice of DPD parameter $a = 90$. [Color figure can be viewed at wileyonlinelibrary.com]

free energy dominates over the contribution of the internal energy) all comonomers are in good solvent conditions. This allows us not to take into account the features of the chemical structure of DPD beads and to select all the repulsion parameters to be the same. In our DPD model we used a single set of interaction parameters for all particles, bonds, and angles. The ratio between the repulsion parameter a, bond strength b, and angle strength c was set to 1:1:0.02 to keep the distribution of ABC and BAB angles (see Fig. 1) in monomers close to the one in MD simulations of monomer melts.[11,14] Equilibrium bond length was set to 0.5, equilibrium angles between bonds – to π. We simulated matrix curing up to conversion degree 0.9 at various values of a, b, and c, with a varied from 12 to 200 and b and c based on the ratio shown above. While curing, the conditions of constant temperature and volume ensemble were used. For the test samples described in this section the probability of triazine formation p_t was set to zero. Then the topologies of all matrices were analyzed in terms of the distribution of simple cycle lengths, first introduced in ref. 25. Simple cycles were shown to become one of the most important characteristics of polymer network graph, as they efficiently describe topological distances between all possible pairs of vertices.[52] We examined the so-called simple cycles, defined as cycles in which the lengths of the paths between any two vertices along the cycle are equal to the topological distances between them. Figure 4 shows part of the distributions with the small cycle length. Weak interaction parameters lead to the peak at cycle length equal to 5, growing from $a \approx 80$. This peak corresponds to bonding of the monomer to itself due to insufficient repulsion between its ending particles. This effect should be avoided, because the excluded volume in atomistic model prevents linking of one end of the monomer with another. Strong interaction parameters result in rapid growth of peak at cycle length 10. This peak corresponds to the presence of interlinked monomer pairs (see insert on Fig. 4) formed due to reduced diffusion rate of the monomers. Large amounts of interlinked monomer pairs lead to enormous local nematic ordering and formation of liquid crystalline clusters in DPD model. The optimum set of DPD parameters thus is $a = b = 90$ and $c = 1.8$. This set makes it possible to avoid both abnormal 5 and 10 length cycles (see thick black line on Fig. 4), and thus was used for the preparation of the samples described below.

MD Simulation Parameters

The molecular dynamics simulations of the created as described in the previous sections fully atomistic phthalonitrile matrices were further performed using the GROMACS[53,54] and the LAMMPS[55] packages to elucidate the influence of the degree of conversion and the way of crosslinking (with and without formation of triazine) on the structural properties. All of the simulated systems contained 32,240 atoms, and at normal pressure $p = 1$ atm and temperature $T = 800$ K had dimensions from 7.6 × 7.6 × 7.6 nm^3 to 8.2 × 8.2 × 8.2 nm^3, depending on the degree and the way of crosslinking. Periodic boundary conditions were applied in all three directions. All equilibration and production runs were performed using pcff[56] force field for interatomic interactions. The same force-field was used in our recent papers (for the simulation of polyisoprene–silica composites[28] and phthalonitrile bulks).[11,14] The non-bonded atoms interacted through LJ 9-6 potential with 1 nm cut-off. The charged atoms interacted through Coulomb potential. The bonded interactions were described with corresponding bond stretching, angle bending, torsion interactions, and improper dihedral potentials. Equilibration and production runs were performed in constant temperature, constant pressure NPT ensemble at a pressure of 1 atm. The systems were firstly equilibrated by MD runs with small timestep of 0.01 fs–1 fs for about 23 ns at $T = 300$–650 K in LAMMPS. In LAMMPS simulations to treat electrostatic interactions the particle–particle particle-mesh method was used. The temperature and pressure were controlled with command "fix npt," with the keyword *iso* meaning that three diagonal components were coupled all together when pressure was computed.[55] The temperature damping parameter was fixed to 100 fs and the pressure damping parameter was chosen to be equal to 1000 fs. Then, the systems were annealed: for 30 ns at $T = 600$ K, for 30 ns at $T = 400$ K, for 30 ns at $T = 800$ K, cooled down to $T = 100$ K at cooling rate of 10 K/ns and cooling step of 100 K, heated up to $T = 800$ K at heating rate of 10 K/ns and heating step of 100 K and, finally, equilibrated for 20 ns at $T = 800$ K (with a time step of 1 or 2 fs, depending on the system) in GROMACS engine. In GROMACS simulations the particle-mesh Ewald method was used for calculating electrostatic interactions. The bond lengths were constrained with the LINCS algorithm.[53] The temperature and pressure were fixed using Berendsen thermostat and barostat, respectively. The same parameters for

thermo- and barostat and for the Ewald summation were used in the recent papers.[14,28] The trajectory was saved every 5 or 10 ps, depending on the system. To calculate glass transition temperature the systems were gradually cooled down from $T = 800$ K to $T = 100$ K at cooling rate of 5 K/ns and cooling step of 20 K for all systems. For highly crosslinked matrices, the cooling rate does not strongly affect the reproducibility of the experimental glass transition temperature.[57]

Estimating Glass Transition Temperature and Coefficient of Linear Thermal Expansion

Glass transition temperature was calculated from changing slopes in the density-temperature dependencies at temperatures varying in the interval 100–700 K. First, all data in the density-temperature dependence was divided into two sets of points in a raw. Each ith set of points was fitted with linear equation $y(x)=a_i x+b_i$. The coefficients a_i, b_i in the corresponding linear fits were calculated using the method of least squares. All possible cases of division were considered with minimum of 2 points in each dataset. Then, we chose the case, for which the functional $F=\sum_{i_1=2}^{N_1}(y(i_1)-a_1x(i_1)-b_1)+\sum_{i_2=2}^{N_2}(y(i_2)-a_2x(i_2)-b_2)$ was minimal. Here, N_1, a_1, b_1 and N_2, a_2, b_2 are number of points and the coefficients of linear fits of the first and second sets of points, respectively. Each of the two chosen datasets, that approximately correspond to the datasets below and above T_g, was further filtered to maximize square correlation coefficient R^2 of linear approximation, with the condition of minimum 4 points in each dataset. Then, in each of the datasets 3 sets of points with maximum R^2 were selected and fitted with linear fits. The corresponding coefficients ($a_{1,i}$, $b_{1,i}$, $a_{2,j}$, $b_{2,j}$, $i = 1,3$, $j = 1,3$) and their root-mean-square errors ($S_{a1,i}$, $S_{b1,i}$, $S_{a2,j}$, $S_{b2,j}$, $i = 1,3$, $j = 1,3$) were calculated using the method of least squares. From the intersection of different pairs of these linear fits 9 values of T_g were then determined, $T_{g,ij}=(-b_{1,i}-b_{2,j})/(a_{1,i}-a_{2,j})$, $i = 1,3$, $j = 1,3$, and the final value of T_g was calculated as their average value $T_g=\frac{1}{9}\sum_{i=1}^{3}\sum_{j=1}^{3}T_{g,ij}$. Errors of the 9 determined values of T_g and of the final value of T_g were estimated as errors of indirect random measurements:

$$S_{T_{g,ij}}=\left(\left(\frac{\partial T_{g,ij}}{\partial a_{1,i}}S_{a1,i}\right)^2+\left(\frac{\partial T_{g,ij}}{\partial b_{1,i}}S_{b1,i}\right)^2+\left(\frac{\partial T_{g,ij}}{\partial a_{2,j}}S_{a2,j}\right)^2+\left(\frac{\partial T_{g,ij}}{\partial b_{2,j}}S_{b2,j}\right)^2\right)^{\frac{1}{2}},$$

$$S_{T_g}=\sum_{i=1}^{3}\sum_{j=1}^{3}\left|\frac{\partial T_g}{\partial T_{g,ij}}S_{T_{g,ij}}\right|=\frac{1}{9}\sum_{i=1}^{3}\sum_{j=1}^{3}|S_{T_{g,ij}}|,\ i=1,3,\ j=1,3.$$

In Figure 5, the two utmost fits for the datasets below and above T_g are shown on the example of the system without triazine of conversion 0.1. The intersections of the pair of fits shown in green lines and the pair of fits shown in black lines determine the lower (388 K) and the upper (400 K) thresholds for estimating T_g, respectively (see Fig. 5). Thus, the geometrically determined value of T_g is equal to 394 ± 6 K, the calculated value of T_g is equal to 395 ± 10 K.

Coefficient of linear thermal expansion (CLTE) at $T = 300$ K and averaged over the interval $T = 313$–363 K was calculated using the formula:

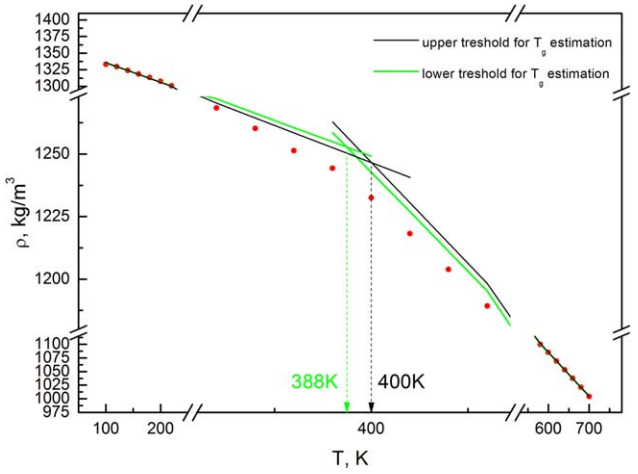

FIGURE 5 The geometrical illustration of how the error of T_g was determined on the example of the system without triazine of conversion 0.1. The green and black dashed vertical arrows indicate the lower (388 K) and the upper (400 K) thresholds for estimating T_g, respectively. [Color figure can be viewed at wileyonlinelibrary.com]

$$\alpha=\frac{1}{L_0}\left(\frac{\partial L}{\partial T}\right)_P=-\frac{1}{3\rho_0}\left(\frac{\partial \rho}{\partial T}\right)_P.$$

EXPERIMENTAL

Materials and Methods

Liquid NMR spectra were run on "Bruker Advance 600" at 600 MHz for ^{1}H, at 151 MHz for ^{13}C and at 162 MHz for ^{31}P NMR with DMSO-d_6 as solvent.

Densities of the cured resins were measured by hydrostatic weighing using *n*-octane as the immersion liquid. The densities of three samples were measured for every treatment time, and the average value is reported.

The measurements of the CLTE of the cured samples were performed on "Netzsch TMA 402" using an expansion probe. These samples had a size of 4 × 4 × 2 mm^3. The samples were mounted on the TMA and heated up to 200–400 °C at a heating rate of 5 °C/min. The CLTE was determined from the slope of the plot on linear range. The CLTE was measured for two different samples with the same composition, and the average value is reported.

Glass transition of the cured samples was measured by dynamic mechanical analysis and assigned according to ASTM E1640 with accuracy ±4 °C. DMA was performed using TA Instruments DMA Q800 in 3-point Bending regime with frequency 1 Hz and amplitude 40 μm with heating rate of 5 K/min.

Bis(3-(3,4-dicyanophenoxy)phenyl)phenyl phosphate was prepared as described in ref. 2 with yield (84%). ^{1}H NMR (DMSO-d_6, δ ppm): 8.10 (t, 2H, ArH), 7.83 (t, 2H, ArH), 7.55 (t, 2H, ArH), 7.40–7.47 (m, 4H, ArH), 7.22–7.31 (m, 5H, ArH), 7.08–7.15 (m, 4H, ArH). ^{13}C NMR (DMSO-d_6, δ ppm):

160.17 (s), 154.96 (s), 150.78 (s), 149.55 (s), 136.31 (s), 131.92 (s), 130.27 (s), 126.10 (s), 123.21 (s), 122.65 (s), 119.90 (s), 117.63 (s), 117.05 (s), 116.77 (s), 115.75 (s), 115.25 (s), 112.31 (s), 108.92 (s). ^{31}P NMR (DMSO-d_6, δ ppm): −18.16 (s). Calculated for $C_{34}H_{19}N_4O_6P$: C (66.89%), H (3.14%), N (9.18%), P (5.07%). Found: C (66.51%), H (3.25%), N (9.24%), P (5.06%).

Curing Process

To obtain molded plates, the monomer **1** (see Fig. 1) (50 g) was placed into a 250 mL flask, then melted and degassed by stirring under vacuum at 140 °C until homogeneous dark resin was obtained. Then APB (see Fig. 1) (2 g) was added and the mixture was stirred for 20 more minutes at 300 RPM. Next, the mixture was poured into metal mold for measurements of CLTE and density (70 × 70 × 4 mm^3). The molds were placed into an air circulated heated oven and cured at 200 °C for 6 h. Next, the molds were disassembled and the cured plates were cut by milling on a CNC machine according to the measurement requirement, and samples were post-cured under inert atmosphere at 250 °C for 6 h, at 300 °C for 6 h, and at 350 °C for 6 h at heating rate of 2 °C/min.

RESULTS AND DISCUSSION

In this section, we present the results of applying the methodology described above to the case of standard phthalonitrile resin based on monomer **1** and initiator APB (see Fig. 1) and compare them with the obtained experimental data (see Table 1).

In general, the computational study consists of several consequential processes "DPD-curing → reverse mapping → MD studying." In our research, we studied structural properties of a set of atomistic configurations of the same sample at various conversion degrees. In addition to conversion degree the probability of triazine formation was the second variable for our network structure. In this paper, we present two limiting cases of absence of triazine formation, $p_t = 0$, and maximum amount of triazine, $p_t = 1$, for showing the strongest possible influence of triazine formation on the network structure and properties. Results for all other p_t values should lie in between these two limiting cases.

Figure 6(a) shows the general view of all obtained temperature-density dependencies after the preliminary equilibration procedure described above and at the optimum cooling rate of 5 K/ns. One can see a set of smooth nested curves which itself partly indicates the correct choice of selected methodology and simulation parameters. Also, the CLTEs observed for the systems of conversion 0.9 at $T = 300$ K are approximately equal to $5.4{\cdot}10^{-5}$ K^{-1} and CLTEs averaged over the temperature range 313–363 K are approximately equal to $4.9{\cdot}10^{-5}$ K^{-1} and $5.5{\cdot}10^{-5}$ K^{-1} (for the systems without and with triazine, respectively). These values correspond well to the experimental values, lying in the range of $4.19{\cdot}10^{-5}$–$5.89{\cdot}10^{-5}$ K^{-1} (see Table 1). Figure 6(b) represents the vertical cut section of Figure 6(a),

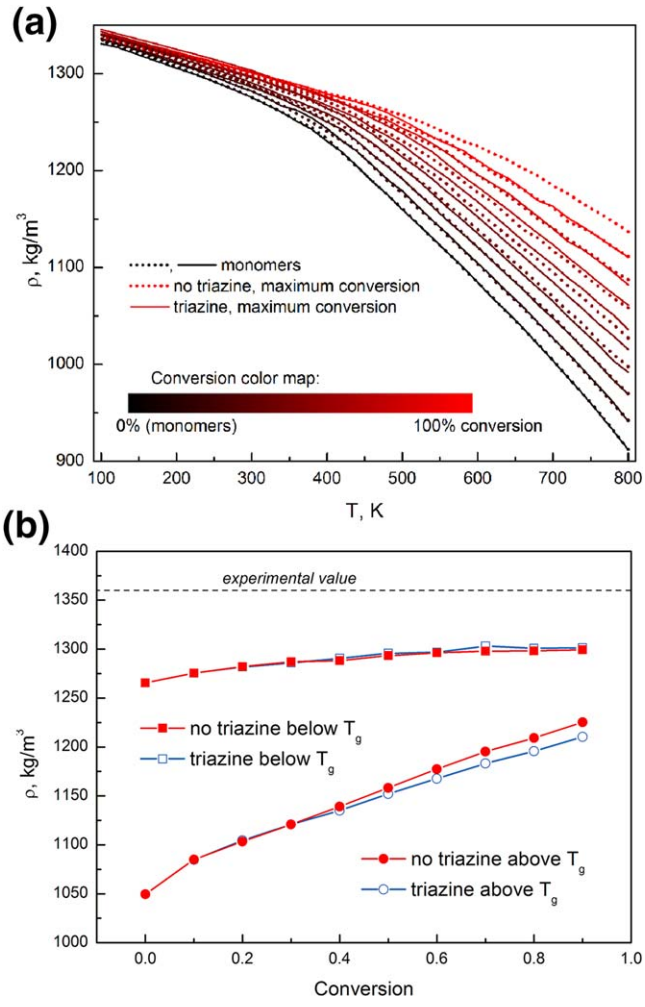

FIGURE 6 (a) The temperature dependencies of the system density for systems with and without triazine and of various conversions. (b) The system density as a function of conversion degree below (300 K) and above (600 K) the glass transition temperature for systems with and without triazine. The observed experimental value of 1360 kg/m^3 at $T = 293$ K is marked as a horizontal dashed line. [Color figure can be viewed at wileyonlinelibrary.com]

namely, the system density as a function of conversion degree well below (300 K) and above (600 K) the glass transition temperature. This plot shows that in a glassy state the system density is almost independent on the conversion degree, and there is only small increase in system density upon the increase in conversion. Also, there is no difference on the details of curing process: data for both systems with triazine and without triazine coincide. We note here that values of system density obtained from MD simulations are about 4% lower than the observed experimental values [1360 kg/m^3 in curing temperature range of 200–300 °C, marked as a horizontal dashed line in Fig. 6(b), see Table 1]. This situation is typical for atomistic simulation of complex liquids and polymer systems (both melts and networks) and is originated from not ideally equilibrated molecular conformations. It is believed that the small mismatch of density is

suitable for MD simulations and will not affect other characteristics, including T_g. The dependence of the system density on conversion degree at elevated temperature, where the system is unfrozen and amorphous, is much more pronounced and one can observe small but clearly visible differences between the systems with and without triazine. Triazine-containing systems are less dense at conversion degrees over 0.4. The origin of such differences is discussed below.

The influence of curing process on the network size and glass transition temperature was studied. Figure 7(a) presents the system gel fraction for systems with and without triazine and the normalized amount of triazine as a function of conversion degree according to DPD simulations. The system gel fraction was calculated as a ratio of a number of monomer units in single maximal cluster divided by overall number of monomer units. The size of maximum cluster sharply grows at conversion degree ~0.2, where sol–gel transition takes place (maximum cluster growth gradient has a maximum). Normalized amount of triazine [dashed line on Fig. 7(a)] was calculated as the ratio between the actual number of triazine units and its theoretical maximum (2/3 of number of monomers). One can see that the amount of triazine grows almost linearly with the increase in the conversion degree. Figure 7(b) shows the dependence of the glass transition temperature on the conversion degree according to MD simulations. Calculated values of T_g are plotted with squares ($p_t = 0$) and circles ($p_t = 1$) with corresponding error bars, solid lines represent the simple sigmoidal fits and should be considered mainly as an eye-guide curves. At conversion degrees above 0.3 the system without triazine tends to higher T_g values, but due to high error values it cannot be quantified with confidence. The values of T_g from MD simulations [see Fig. 7(b)] are generally consistent with experimental data (Table 1). The comparison of these data shows that (i) the lowest curing temperature (200 °C) results in only small conversion degree of 0.3–0.4, regarding the simulations data; (ii) at higher curing temperatures (250–300 °C), the conversion degree of the system reaches much higher values, up to 0.8–0.9; (iii) at the highest curing temperature (350 °C) presumably more complex reactions occur, as the value of T_g obtained experimentally becomes sufficiently higher than the one in MD simulations.

To analyze the difference between two curing mechanisms we also calculated distribution of simple cycles for systems with and without triazine at maximum conversion (ca. 0.95 for both systems), see Figure 8. This characteristic makes it possible to understand the overall network connectivity and its dispersity. One can see the very pronounced difference between the systems with and without triazine. We can conclude that the overall network structure is much denser in the system without triazine. Again, these differences are easily explained by the fact that during triazine formation the growing chain disengages from the triazine unit formed and continues to grow separately. This is why we can clearly see that the network structures of the systems with and without

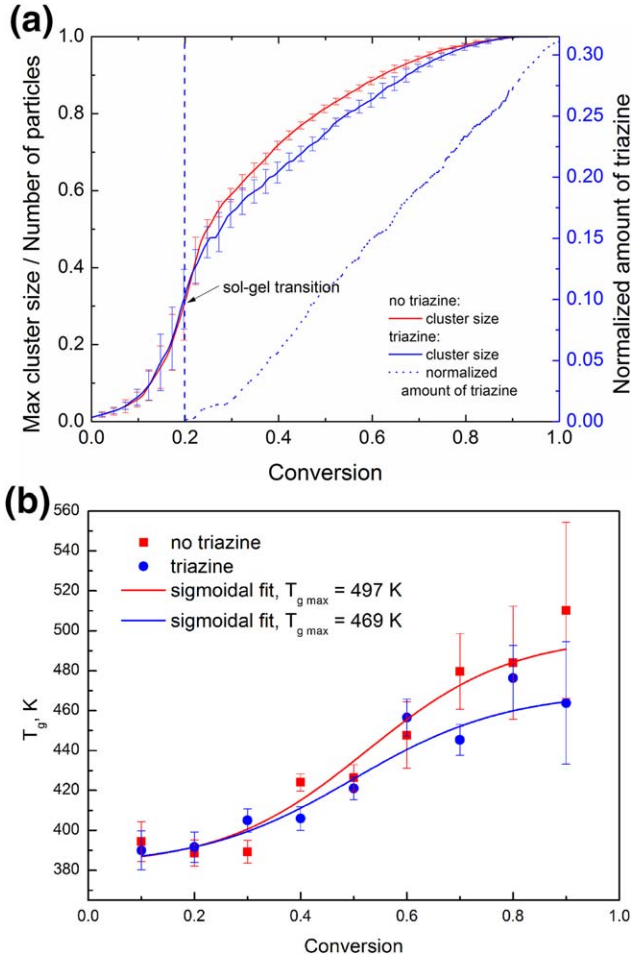

FIGURE 7 (a) The calculated size of the gel fraction for systems with and without triazine and normalized amount of triazine as a function of conversion degree according to DPD simulations. (b) The glass transition temperature as a function of conversion degree for systems with and without triazine according to MD simulations. [Color figure can be viewed at wileyonlinelibrary.com]

triazine are very different, while gelation and further vitrification are very similar.

Thus, we observe here an interesting decoupling of network topology and vitrification transition: despite different curing processes and considerable differences in final network structure there are very small differences in densities below T_g, coefficients of linear thermal expansion and behavior of glass transition temperature. That is, the mean length of simple cycles in triazine-containing sample is almost twice larger than in the triazine-free sample. But the glass transition temperature at high conversion degree is almost the same, with respect to large error values at elevated conversions.

We believe that such counterintuitive observation in this particular system is explained by the fact that vitrification is a very local process and hardly depends on long-range network structure. It was shown before in[6–8,11] that the glass transition in phthalonitrile melts is mainly affected by

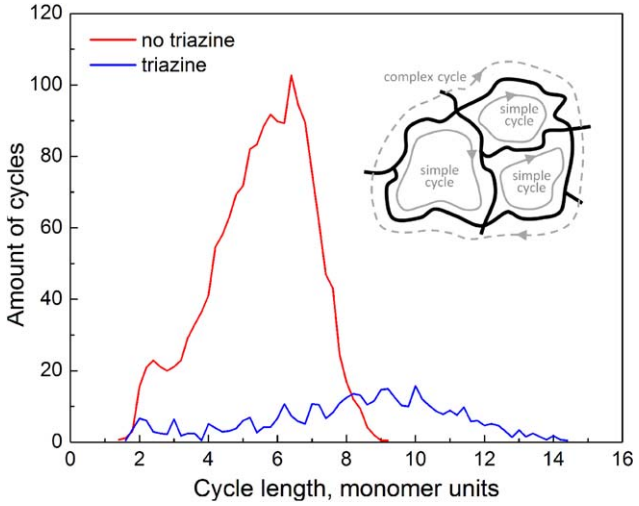

FIGURE 8 Distribution of simple cycles over the generated network topology at maximum conversion degree (ca. 0.95) for systems with and without triazine, averaged over 10 samples. [Color figure can be viewed at wileyonlinelibrary.com]

monomer rigidity and conformational entropy. As soon as we fix the monomer position by linking it to the main gel cluster there is hardly any way to utilize its possible movements and, thus, system vitrification weakly depends on further network details.

We have to mention also, that to the best of our knowledge, the dependence of the glass transition temperature on conversion degree and curing details [Fig. 7(b)] was not presented in literature for phthalonitrile resins before. Thus, computer simulations here are the only instrument for studying details of curing process and for understanding correlations between network topology and system properties.

From comparison of the results of computer simulation and the experimental data it is seen that the developed model reproduces the temperature properties of the material formed at low crosslinking temperatures of 473 K and 523 K. Thus, the model based on the simple polymerization mechanism makes it possible to construct samples of material with properties close to experimental ones. However, the higher densities are left unreachable for this model. We do not think that the problem is related to the valence-force field (VFF). The force-field used is a well-parameterized *ab initio*-based force field of Class II (including such VFFs as CFF91, PCFF, CFF, COMPASS), capable to reproduce the properties of many organic substances and, in particular, polymers.[25,27,28,58] For example, it well reproduces the physical properties of filled elastomer nanocomposites.[27] Thus, we believe that the discrepancy with the experimental results is determined by other factors, as the model reproduces quite well the properties of the studied material obtained in low-temperature crosslinking.

We think that the cause for the unsatisfactory simulation results for the high-density samples is the use of the NVT ensemble at the stage of crosslinking. The use of the NVT ensemble does not allow to reproduce the shrinkage of the material upon high-temperature curing. This problem is discussed in the work on epoxy resins by Yarovsky and Evans,[17] in the work on filled elastomer nanocomposites by Pavlov and Khalatur[27] and in the review of Li and Strachan.[57] The satisfactory reproducibility of the experimental results for the phthalonitrile systems obtained in the low-temperature crosslinking reaction is due to the fact that in this case the density of the experimental samples does not increase strongly. This can be explained by the formation of network structures with long subchains of ~3 to 5 monomers (Fig. 8), that compensates the use of the NVT ensemble. However, at high temperatures there is a significant increase in the density of experimental samples, and the network structures with shorter sub-chains should form. In this case, the NVT ensemble does not allow the corresponding topological structures to form. In further studies, we are going to improve our approach by introducing a barostat into our DPD model.

CONCLUSIONS

To conclude, we formulate here our main achievements:

1. A multiscale procedure for simulating complex curing process of polymer matrices is developed and tested. The advantage of this procedure is that it is automatic process, which does not require manual processing of calculated at different scales intermediate data.
2. The procedure is applied to the case of phthalonitrile resin based on low-melting monomer *bis(3-(3,4-dicyanophenoxy)phenyl)phenyl phosphate* with varied probability to form triazine units while crosslinking, which mimics high-temperature and low-temperature realistic curing processes. We obtained realistic values of the density, coefficients of linear thermal expansion and glass transition temperatures. The dependence of the glass transition temperature on the conversion degree correlates well with the sol–gel transition in the network structure.
3. The topology of the formed resin network is studied at different curing regimes; it is shown that the disposition at formation of triazine units leads to significant differences in network topology: triazine-containing networks are much sparser in comparison with triazine-free matrices of the same conversion degree in terms of simple cycle size.
4. Despite noticeable differences in network topology, the glass transition temperatures and coefficients of linear thermal expansion for different crosslinking mechanisms are very similar. It can only be assumed that the systems without triazine at maximum conversion have slightly higher glass transition temperatures. The reason for that is that the glass transition is the very local process and complex network topology after formation of gel fraction can hardly affect it.

We believe that the presented methodology is universal, that is, suitable without significant changes to almost all polymer curing systems. It could be applied to still not synthesized compounds for studying their structural and mechanical properties during *in silico* experiments and for pre-selecting the set of most promising candidates. While the computational resources have been rapidly growing during past decades, computational screening of artificial chemical materials is the general trend nowadays.[59] For more comprehensive characterization of cured materials, it will be interesting to predict not only thermal expansion behavior and glass transition chemistry, but also mechanical properties at glassy state, both static and dynamic. In addition, we note here that the presented methodology can work also for the case of less-crosslinked materials, that is, elastomers and polymer gels. It is an intriguing feature to apply the same approach to yet unsynthesized elastomeric materials, for example, materials for tire applications, and to test their thermomechanical properties. The network topology and entanglements will play much more important role in a less-crosslinked materials and it is possible to explore their mechanical behavior in coarse-grained DPD simulations.[24]

ACKNOWLEDGMENTS

The reported study was funded by RFBR and Moscow City Government according to the research project № 15–31-70007 "mol_a_mos" and by RFBR according to the research project № 16–33-60215 "mol_a_dk." The research is carried out using the equipment of the shared research facilities of HPC computing resources at Lomonosov Moscow State University.[60]

REFERENCES AND NOTES

1 A. V. Babkin, E. M. Erdni-Goryaev, A. V. Solopchenko, A. V. Kepman, V. V. Avdeev, *Polym. Adv. Technol.* **2016**, *27*, 774.

2 S. E. Evsyukov, T. Pohlmann, H. D. Stenzenberger, *Polym. Adv. Technol.* **2015**, *26*, 574.

3 H. R. Lubowitz, C. H. Sheppard, Polyimide oligomers and blends and method of curing. U.S. Patent 5,116,935, **1992**.

4 Y. Ishida, T. Ogasawara, R. Yokota, *High Perform. Polym.* **2006**, *18*, 727.

5 M. Selladurai, P. R. Sundararajan, M. Sarojadevi, *Chem. Eng. J.* **2012**, *203*, 333.

6 B. A. Bulgakov, A. V. Sulimov, A. V. Babkin, D. V. Afanasiev, A. V. Solopchenko, E. S. Afanaseva, A. V. Kepman, V. V. Avdeev, *Mendeleev Commun.* **2017**, *27*, 257.

7 B. A. Bulgakov, A. V. Sulimov, A. V. Babkin, I. A. Timoshkin, A. V. Solopchenko, A. V. Kepman, V. V. Avdeev, *J. Compos. Mater.* **2017**, in press, DOI:10.1177/0021998317699452.

8 A. V. Babkin, E. B. Zodbinov, B. A. Bulgakov, A. V. Kepman, V. V. Avdeev, *Eur. Polym. J.* **2015**, *66*, 452.

9 C. S. Marvel, J. H. Rassweiler, *J. Am. Chem. Soc.* **1958**, *80*, 1197.

10 X. Peng, H. Sheng, H. Guo, K. Naito, X. Yu, H. Ding, X. Qu, Q. Zhang, *High Perform. Polym.* **2014**, *26*, 837.

11 B. A. Bulgakov, A. V. Babkin, P. B. Dzhevakov, A. A. Bogolyubov, A. V. Sulimov, A. V. Kepman, Y. G. Kolyagin, D. V. Guseva, V. Y. Rudyak, A. V. Chertovich, *Eur. Polym. J.* **2016**, *84*, 205.

12 A. V. Babkin, E. B. Zodbinov, B. A. Bulgakov, A. V. Kepman, V. V. Avdeev, *Polym. Sci. Ser. B* **2016**, *58*, 298.

13 P. B. Dzhevakov, R. F. Korotkov, B. A. Bulgakov, A. V. Babkin, A. V. Kepman, V. V. Avdeev, *Mendeleev Commun.* **2016**, *26*, 527.

14 D. V. Guseva, V. Y. Rudyak, A. V. Chertovich, *J. Chem. Phys.* **2016**, *145*, 144503-1.

15 P. J. Hoogerbrugge, M. V. A. Koelman, *Europhys. Lett.* **1992**, *19*, 155.

16 M. V. A. Koelman, P. J. Hoogerbrugge, *Europhys. Lett.* **1993**, *21*, 363.

17 I. Yarovsky, E. Evans, *Polymer* **2002**, *43*, 963.

18 D. R. Heine, G. S. Grest, C. D. Lorenz, M. Tsige, M. J. Stevens, *Macromolecules* **2004**, *37*, 3857.

19 C. Wu, W. Xu, *Polymer* **2006**, *47*, 6004.

20 J. Baschnagel, K. Binder, P. Doruker, A. A. Gusev, O. Hahn, K. Kremer, W. L. Mattice, F. Muller-Plathe, M. Murat, W. Paul, S. Santos, W. W. Suter, V. Tries, *Adv. Polym. Sci.* **2000**, *152*, 41.

21 T. C. Clancy, *Polymer* **2004**, *45*, 7001.

22 P. V. Komarov, C. Yu-Tsung, C. Shih-Ming, P. G. Khalatur, P. Reineker, *Macromolecules* **2007**, *40*, 8104.

23 H. Liu, M. Li, Z.-Y. Lu, Z.-G. Zhang, C.-C. Sun, T. Cui, *Macromolecules* **2011**, *44*, 8650.

24 A. A. Gavrilov, A. V. Chertovich, P. G. Khalatur, A. R. Khokhlov, *Macromolecules* **2014**, *47*, 5400.

25 A. A. Gavrilov, P. V. Komarov, P. G. Khalatur, *Macromolecules* **2015**, *48*, 206.

26 A. S. Pavlov, P. G. Khalatur, *Chem. Phys. Lett.* **2016**, *653*, 90.

27 A. S. Pavlov, P. G. Khalatur, *Soft Matter* **2016**, *12*, 5402.

28 D. V. Guseva, P. V. Komarov, A. V. Lyulin, *J. Polym. Sci. B: Polym. Phys.* **2016**, *54*, 473.

29 A. C. T. van Duin, S. Dasgupta, F. Lorant, W. A. Goddard, *J. Phys. Chem. A* **2001**, *105*, 9396.

30 J. D. Deetz, R. Faller, *J. Phys. Chem. B* **2014**, *118*, 10966.

31 V. Y. Rudyak, A. A. Gavrilov, D. V. Guseva, A. V. Chertovich, *Macromol. Theory Simul.* **2017**, *26*, 1700015-1.

32 R. Yang, K. Li, L. Tong, K. Jia, X. Liu, *J. Polym. Res.* **2015**, *22*, 210-1.

33 S. Ji, P. Yuan, J. Hu, R. Sun, K. Zeng, G. Yang, *Polymer* **2016**, *84*, 365.

34 D. Augustine, D. Mathew, C. P. R. Nair, *Eur. Polym. J.* **2015**, *71*, 389.

35 L. Sheng, C. Yin, J. Xiao, *RSC Adv.* **2016**, *6*, 22204.

36 L. E. Nielsen, *Crosslinking-Effect on Physical Properties of Polymers*; Monsanto Research Corporation: St. Louis, MO, **1968**.

37 A. Shefer, M. Gottlieb, *Macromolecules* **1992**, *25*, 4036.

38 J. Bicerano, R. L. Sammler, C. J. Carriere, J. T. Seitz, *J. Polym. Sci. B: Polym. Phys.* **1996**, *34*, 2247.

39 T. Sasaki, T. Uchida, K. Sakurai, *J. Polym. Sci. B: Polym. Phys.* **2006**, *44*, 1958.

40 J. Liu, D. Cao, L. Zhang, *J. Chem. Phys.* **2009**, *131*, 034903-1.

41 C. Li, A. Strachan, *Polymer* **2010**, *51*, 6058.

42 H. Lin, T. Kai, B. D. Freeman, S. Kalakkunnath, D. S. Kalika, *Macromolecules* **2005**, *38*, 8381.

43 H. Yagyu, T. Utsumi, *Comput. Mater. Sci.* **2009**, *46*, 286.

44 Y. Lan, D. Li, J. Zhai, R. Yang, *Ind. Eng. Chem. Res.* **2015**, *54*, 3563.

45 P. Espanol, P. Warren, *Europhys. Lett.* **1995**, *30*, 191.

46 R. D. Groot, P. B. Warren, *J. Chem. Phys.* **1997**, *107*, 4423.

47 R. D. Groot, T. M. Madden, *J. Chem. Phys.* **1998**, *108*, 8713.

48 A. V. Berezkin, Y. V. Kudryavtsev, *Macromolecules* **2011**, *44*, 112.

49 DPDChem-Software, https://www.researchgate.net/project/DPDChem-Software, **2017**.

50 J. Zhang, J. Su, Y. Ma, H. Guo, *J. Phys. Chem. B* **2012**, *116*, 2075.

51 L. Larini, J. E. Shea, *J. Phys. Chem. B* **2012**, *116*, 8337.

52 J. L. Gross, J. Yellen, P. Zhang, *Handbook of Graph Theory*, 2nd ed.; CRC Press: Boca Raton, FL, **2013**.

53 D. Van der Spoel, E. Lindahl, B. Hess, A. R. Van Buuren, E. Apol, P. J. Muelenhoff, D. P. Tielemann, A. L. T. M. Sijbers, K. A. Feenstra, R. Van Drunen, H. J. C. Berendsen, Gromacs User Manual Version 4.5.6, www.gromacs.org, **2010**.

54 D. Van Der Spoel, E. Lindahl, B. Hess, G. Groenhof, A. E. Mark, H. J. Berendsen, *J. Comput. Chem.* **2005**, *26*, 1701.

55 LAMMPS Users Manual 24 Jul 2017 Version, http://lammps.sandia.gov – Sandia National Laboratories, Sandia Corporation, **2017**.

56 H. Sun, S. J. Mumby, J. R. Maple, A. T. Hagler, *J. Am. Chem. Soc.* **1994**, *116*, 2978.

57 C. Li, A. Strachan, *J. Polym. Sci. B: Polym. Phys.* **2015**, *53*, 103.

58 P. V. Komarov, P. G. Khalatur, A. R. Khokhlov, *Beilstein J. Nanotechnol.* **2013**, *4*, 567.

59 A. Jain, S. P. Ong, G. Hautier, W. Chen, W. D. Richards, S. Dacek, S. Cholia, D. Gunter, D. Skinner, G. Ceder, K. A. Persson, *APL Mater.* **2013**, *1*, 011002-1.

60 Research Computing Center of Lomonosov Moscow State University, http://hpc.msu.ru (accessed November 15, **2017**).